© 2018. Published by The Company of Biologists Ltd | Journal of Experimental Biology (2018) 221, jeb149583. doi:10.1242/jeb.149583

REVIEW

Biomechanics of swimming in developing larval fish

Cees J. Voesenek, Florian T. Muijres and Johan L. van Leeuwen*

ABSTRACT

Most larvae of bony fish are able to swim almost immediately after hatching. Their locomotory system supports several vital functions: fish larvae make fast manoeuvres to escape from predators, aim accurately during suction feeding and may migrate towards suitable future habitats. Owing to their small size and low swimming speed, larval fish operate in the intermediate hydrodynamic regime, which connects the viscous and inertial flow regimes. They experience relatively strong viscous effects at low swimming speeds, and relatively strong inertial effects at their highest speeds. As the larvae grow and increase swimming speed, a shift occurs towards the inertial flow regime. To compensate for size-related limitations on swimming speed, fish larvae exploit high tail beat frequencies at their highest speeds, made possible by their low body inertia and fast neuromuscular system. The shifts in flow regime and body inertia lead to changing functional demands on the locomotory system during larval growth. To reach the reproductive adult stage, the developing larvae need to adjust to and perform the functions necessary for survival. Just after hatching, many fish larvae rely on yolk and need to develop their feeding systems before the yolk is exhausted. Furthermore, the larvae need to develop and continuously adjust their sensory, neural and muscular systems to catch prey and avoid predation. This Review discusses the hydrodynamics of swimming in the intermediate flow regime, the changing functional demands on the locomotory system of the growing and developing larval fish, and the solutions that have evolved to accommodate these demands.

KEY WORDS: Cost of transport, Energetics of locomotion, Escape manoeuvre, Fluid dynamics, Muscle development, Zebrafish

Introduction

After hatching from the egg, most bony fish continue life as a larva, a few millimetres in length, that needs to survive autonomously. They have to hunt prey to gather resources for their growth and development, disperse, and escape from predators. This requires the larvae to swim effectively almost immediately after hatching. They generally use an undulatory swimming style (see Glossary), characterised by caudally directed waves of lateral bending of their body and tail. As the fish grow from larvae into juveniles, functional demands on the locomotory system change, requiring larval fish to adapt their locomotory system continuously to these varying requirements.

The fluid-dynamic regimes for swimming fish are defined by the dimensionless Reynolds number (*Re*; see Glossary) (e.g. Bainbridge, 1960), given by:

$$Re = \frac{\rho \bar{v} l}{\mu} = \frac{\bar{v} l}{\nu}\ , \qquad (1)$$

where ρ is fluid density, $\bar{v}$ is mean swimming speed, l is body length, μ is dynamic viscosity and ν is kinematic viscosity (see Glossary). The Reynolds number expresses the ratio of contributions of inertial and viscous forces to a fluid-dynamic phenomenon, which is crucial to its dynamics. Viscosity is associated with friction between fluid particles, and inertia (see Glossary) is the tendency of mass to keep the same velocity in the absence of external forces. Very low *Re* values ($Re \ll 1$) are associated with the viscous flow regime (see Glossary), where inertia can be ignored. Much larger *Re* values ($Re \gtrsim 2000$) indicate that inertia dominates. In the intermediate flow regime ($1 \lesssim Re \lesssim 2000$) (see Glossary), there is a gradual transition from viscosity-dominated flow at $Re \approx 1$ to inertia-dominated flow at $Re \approx 2000$.

Small fish larvae ($l \lesssim 5$ mm) operate in the intermediate flow regime over most of their range of swimming speeds, whereas larger fish larvae enter the inertial regime (see Glossary) at their highest swimming speeds (e.g. Fuiman and Webb, 1988; Müller and Van Leeuwen, 2004). In the intermediate flow regime, fish larvae have to deal with relatively strong viscous effects at low swimming speeds, whereas, at their highest speeds, inertial effects come to dominate. The changing hydrodynamic circumstances affect the production of fluid-dynamic forces. Hence, demands on the locomotory system change with swimming speed. Because the larvae need to swim throughout a range of speeds, they cannot adapt to a specific hydrodynamic regime and thus need to compromise in morphology, physiology and muscle control to accommodate the varying functional demands.

Bony fish larvae change shape considerably over development (Fig. 1), but the morphology of early larval stages of most species is surprisingly similar. When the larvae hatch, they have an elongated body surrounded by a continuous finfold (see Glossary) behind the head and yolk sac (Kendall et al., 1984). These similarities might indicate adaptations to common developmental constraints and/or common problems in locomotion, feeding and respiration. As the larvae grow and develop into juveniles, the body shapes of the different species diverge to prepare them for their adult lifestyle and swimming styles. For example, flatfish such as halibut change from a yolk-sac-bearing larva to a pelagic suction feeder to an asymmetric benthic flatfish (Fig. 1B) (Osse and Van den Boogaart, 1997). In addition to the changing hydrodynamic regime, these changes over the life history of the fish also result in changing functional demands.

This Review addresses the locomotory challenges that larval fish have to cope with, as well as the evolved solutions to the associated functional demands. We discuss the kinematics, fluid dynamics and energetics of swimming, and how the muscles of fish larvae are adapted to power swimming in the intermediate flow regime. Furthermore, we examine the functions supported by the locomotory system and how fish larvae have adapted to the demands derived from these functions (see Fig. 2 for an overview). Cruising is essential for many fish larvae, to disperse or to avoid dispersal caused by environmental flow (discussed in the section Cruising and dispersal). An important factor for survival is escape

Experimental Zoology Group, Wageningen University, PO Box 338, NL-6700 AH Wageningen, The Netherlands.

*Author for correspondence (johan.vanleeuwen@wur.nl)

C.J.V., 0000-0002-5467-8963; F.T.M., 0000-0002-5668-0653; J.L.v.L., 0000-0002-4433-880X

Journal of Experimental Biology (2018) 221, jeb149583. doi:10.1242/jeb.149583

List of symbols and abbreviations

A	peak-to-peak tail-beat amplitude
CFD	computational fluid dynamics
CoM	centre of mass
CoT	cost of transport
$\bar{D}$	cycle-averaged drag
dpf	days post-fertilisation
f	tail beat frequency
l	body length
$\bar{P}_{input}$	cycle-averaged input power
$\bar{P}_{output}$	cycle-averaged output power
PIV	particle image velocimetry
PTV	particle tracking velocimetry
Re	Reynolds number
SR	sarcoplasmic reticulum
St	Strouhal number
$\bar{T}$	cycle-averaged thrust
$\bar{v}$	cycle-averaged swimming speed
η	Froude efficiency
μ	dynamic viscosity
ν	kinematic viscosity
ρ	density of water

Glossary

Anguilliform
Swimming mode in which undulations occur along a large part of the body.
Carangiform
Swimming mode in which undulations occur mainly near the tail.
Finfold
Larval fin structure surrounding almost the complete body behind the head.
Inertia
Resistance to changes in velocity.
Inertial flow regime
Hydrodynamic regime where inertia dominates; $Re \gtrsim 2000$.
Intermediate flow regime
Hydrodynamic regime where both inertia and viscosity are important; $1 \lesssim Re \lesssim 2000$.
Labriform
Swimming mode in which mainly the pectoral fins are used for propulsion.
Lateral line
Sensory organ for flow detection.
Particle image velocimetry (PIV)
Velocity measurement technique based on cross-correlation of particle images.
Particle tracking velocimetry (PTV)
Velocity measurement technique based on tracking of particles in video frames.
Reynolds number (*Re*)
Ratio between inertial and viscous forces in a fluid (dimensionless number).
Strouhal number (*St*)
Ratio between average lateral tail speed and forward swimming speed (dimensionless number).
Subcarangiform
Swimming mode between anguilliform and carangiform.
Thunniform
Swimming mode in which undulations are confined mostly to the tail.
Undulatory
Using waves of curvature along the body.
Viscosity
Resistance of a fluid to deform under stress.
Viscous flow regime
Hydrodynamic regime where viscosity dominates; $Re \lesssim 1$.

from predators, requiring the locomotory system to respond quickly and accelerate the fish strongly (discussed in the section Escaping predators). Fish larvae need to swim to find and hunt prey after they exhaust their yolk, which requires accurate control to aim their strikes (discussed in the section Hunting and feeding). Swimming also supports respiration by renewing the diffusive boundary layer of gases and ions (e.g. Green et al., 2011), and helps to maintain and control body orientation (e.g. Ehrlich and Schoppik, 2017); for reasons of space, we do not discuss these two functions. Finally, we provide perspectives for possible future research.

Body kinematics

Swimming kinematics are produced by a complex interaction between internal body mechanics and fluid mechanics (e.g. McMillen and Holmes, 2006; Tytell et al., 2010). The muscle system of the fish generates forces that cause body deformations. The resulting motion produces a flow field in the surrounding water, creating a fluid-dynamic force distribution on the skin. In turn, these forces change the loading on the fish, and with it the deformation of the body. Again, this deformation couples back to the fluid forces, creating a loop of interactions between the water and the body of the fish. These mechanical interactions determine the changes in body shape and motion of the fish through the water.

To study these complex interactions, swimming kinematics (i.e. body shape, position and orientation) need to be determined in detail. Historically, this has been performed mostly by tracking the two-dimensional (2D) movements of the body centreline and centre of mass (CoM) in a horizontal plane from a single, vertically oriented movie camera (e.g. Fig. 3A; Müller and Van Leeuwen, 2004), but recently more sophisticated multi-camera three-dimensional (3D) tracking systems have been developed (e.g. Butail and Paley, 2012; Voesenek et al., 2016). Results from these new trackers show that swimming motions that appear 2D in a single (bottom or top) camera view often have a large vertical component. For example, a fast-starting larval zebrafish [5 days post-fertilisation (dpf)] produced pitch angles up to 15 deg with respect to the horizontal plane, roll angles up to 30 deg and a considerable vertical speed, demonstrating the necessity of 3D tracking (Voesenek et al., 2016). Also in 3D, kinematics are generally quantified as the movement and lateral curvature of the body centre line, 3D body orientation, and the displacement of the CoM.

The CoM of the fish is important to determine because it is the point that the resultant fluid-dynamic forces and torques act upon (Fig. 3A,C; Van Leeuwen et al., 2015b; Voesenek et al., 2016). The CoM depends on the mass distribution of the fish at every point in time, and it changes with deformation of the fish (Tytell and Lauder, 2008; Van Leeuwen et al., 2015b). The position of the CoM along the body axis for a straight fish is often used to define a body-attached point that can be tracked to estimate the CoM movement during swimming. This might be a reasonable approximation for low-amplitude swimming motions (Xiong and Lauder, 2014), but for high-amplitude motions as found in swimming larvae, the difference with the true CoM is large (Fig. 3A,B; Van Leeuwen et al., 2015b). Hence, for high-amplitude larval swimming, more sophisticated CoM estimation methods are required, such as methods based on a 3D model of the deforming body.

Fish locomotion has been divided into cyclic and acyclic swimming. In cyclic swimming, the kinematics repeat themselves and the cycle-averaged speed is constant. In reality, however, variations between the swimming cycles always occur. Acyclic

Journal of Experimental Biology (2018) 221, jeb149583. doi:10.1242/jeb.149583

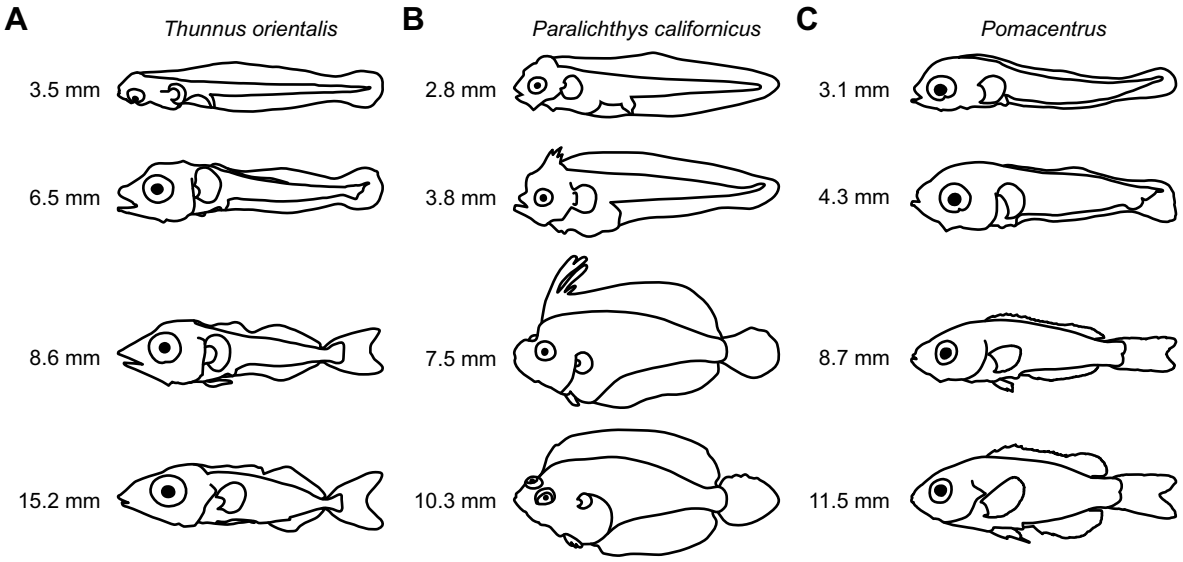

Fig. 1. Line drawings used to illustrate development of external morphology for different species, from yolk-sac larva to juvenile. (A) Thunniform (see Glossary): Pacific bluefin tuna *Thunnus orientalis*, redrawn from Kaji et al. (1996). (B) Subcarangiform (see Glossary): California halibut *Paralichthys californicus*, redrawn from Gisbert et al. (2002). (C) Labriform (see Glossary): a member of the genus *Pomacentrus*, redrawn from Kavanagh et al. (2000). Note that the fish have initially similar shapes that diverge as they develop into juveniles. The body length of each fish is shown to its left.

swimming constitutes a large part of natural swimming motion: turns, escape manoeuvres, feeding strikes and burst-and-coast swimming. Many fish switch from (approximately) cyclic swimming to burst-and-coast swimming early in development (Weihs, 1979; Müller and Van Leeuwen, 2004). Much of the work on the fluid mechanics of fish swimming has focused on (near-) cyclic swimming.

During near-cyclic swimming, many teleost larvae employ an anguilliform swimming style (see Glossary), where the majority of the body makes considerable lateral excursions. An example of this motion is shown in Fig. 3A (Van Leeuwen et al., 2015b), which depicts the kinematics of a 5-dpf zebrafish larva swimming at a speed of approximately 50 body lengths s^{-1}. Compared with adults, the larva shows high-amplitude motion of the whole body (peak-to-peak tail-beat amplitude $A \approx 0.44\ l$ at the tail) at a high frequency (~85 Hz). This anguilliform swimming mode is relatively rare in most fish species at $l > 10$ mm – larvae often change to a more tail-heavy amplitude distribution later in development. Fig. 3D (Osse

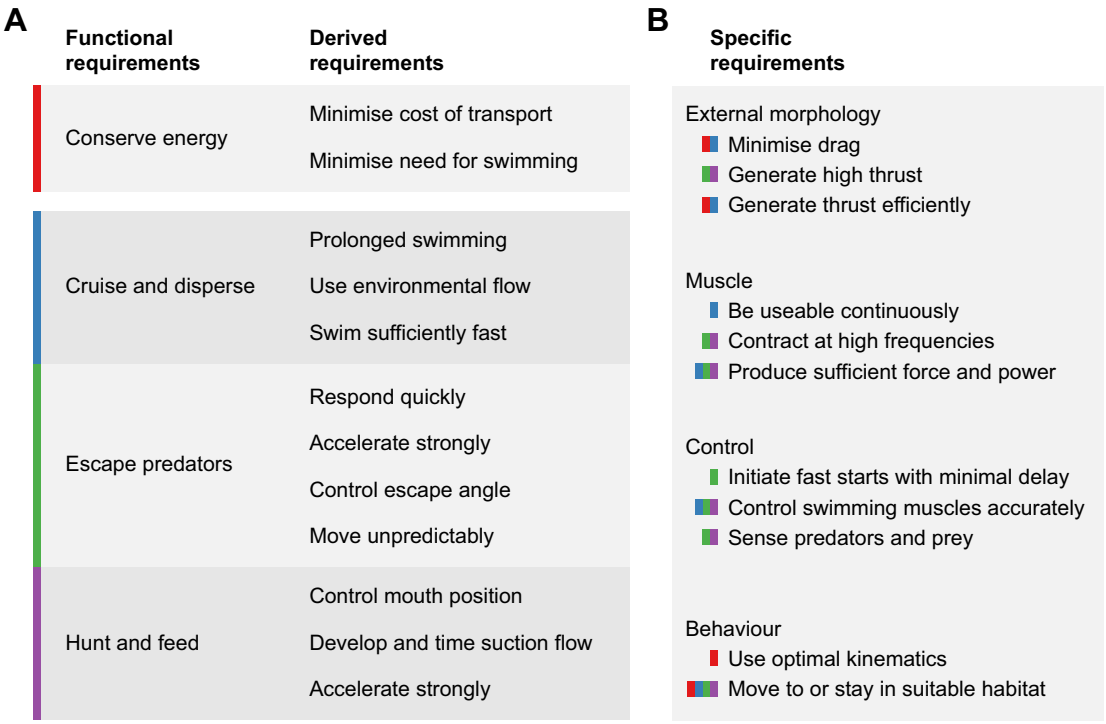

Fig. 2. Requirements on locomotion for developing fish larvae. (A) General requirements on fish larvae, where functional requirements (depicted by different colours) are connected to derived requirements. (B) Specific requirements on the subsystems of the fish. The functional requirement(s) from A that each specific requirement belongs to is indicated by the small coloured rectangle(s).

Journal of Experimental Biology (2018) 221, jeb149583. doi:10.1242/jeb.149583

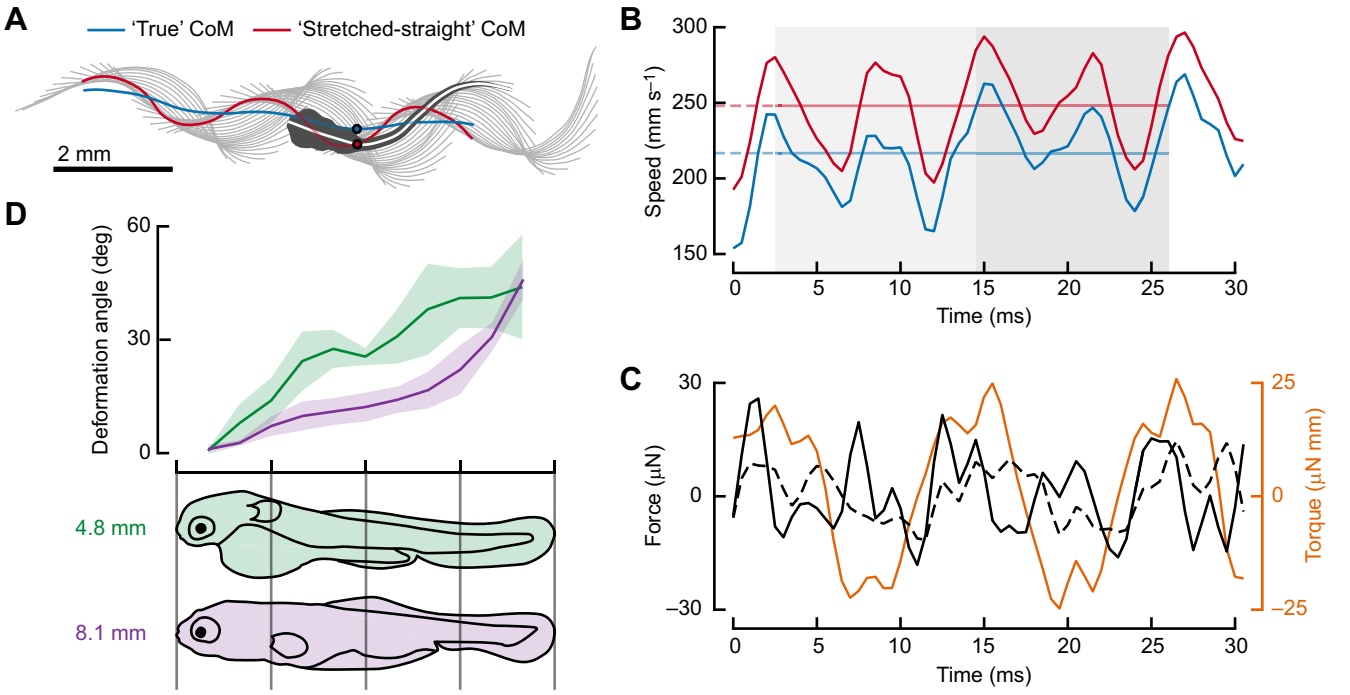

Fig. 3. Swimming kinematics of fish larvae. (A) High-speed-video-derived centreline kinematics (grey), path of the centre of mass (CoM) of a 5 day post-fertilisation (dpf) zebrafish larva based on a body-attached CoM approximation method ('stretched-straight', red), and a more accurate method based on a deforming body model with uniform density ('true', blue). A two-dimensional (2D) projection of the body model is indicated for one time instant, with the two approximations of the CoM indicated with circles. Owing to the large body curvature, the CoM computed with the deforming body model is located outside the body at this instant; the body-attached CoM approximation fails to capture this feature. (B) Speed of the CoM based on the body-attached approximation (red) and the deforming body model (blue). The grey blocks indicate the two swimming cycles, for which the tail-beat averaged speed (horizontal lines) is calculated; this speed is 15% higher for the body-attached approximation (red) than for the deforming body model (blue). (C) Resultant forces (black) and yaw torque (orange) on the CoM, calculated with inverse dynamics. The forces are given in the direction of the instantaneous velocity vector (solid) and perpendicular to it (dashed). Data for A–C are from Van Leeuwen et al. (2015a,b). (D) Change of maximum deformation angle amplitude for two carp larvae, one with a body length of 4.8 mm (green) and the other 8.1 mm (purple). Standard deviations are indicated by the shaded area. The deformation angle is defined as the angle between successive, straight equal-length segments ('virtual body segments') along the central axis. Sketches of larvae are redrawn and data are from Osse and Van den Boogaart (2000).

and Van den Boogaart, 2000) shows the amplitude envelope of the deformation angle between successive 'virtual body segments' for a just-hatched carp larva (4.8 mm) and a larger larva (8.1 mm). The just-hatched larva bends strongly along a large part of the body, whereas the older larva confines large amplitudes to the tail.

Fluid dynamics

Analyses of the hydrodynamic forces on the fish are important for understanding swimming. The flow field surrounding the fish creates time-dependent pressure and shear-stress distributions on the skin. When integrated over the body, these distributions provide a resultant force and torque, resulting in linear and angular accelerations. It is common to divide the resultant force into thrust and drag, where thrust propels the fish, whereas drag opposes its motion. In engineering, drag is defined in the direction of the oncoming flow, and thrust is opposed to it (Anderson, 2001). In many engineering cases, the propulsive system is clearly separate from the body, so drag can easily be distinguished from thrust: drag acts on the body and thrust is produced by the propulsive system. However, for larval fish that undulate their whole body, this distinction is difficult to make (Schultz and Webb, 2002). A large part of the body surface contributes to both forward and backward forces, depending on the phase in the swimming cycle (Fig. 4A,B; Li et al., 2016). Almost no part of the body uniquely contributes to thrust or drag over a complete tail beat cycle, except the head, which almost exclusively experiences drag. Efforts were made to define drag and thrust on an undulating body, for example by separating friction forces from inertia forces (Chen et al., 2011), by estimating thrust from the body motion with a fluid-dynamic model (Webb et al., 1984) or by separating forward- and backward-acting forces (Fig. 4D–F; Li et al., 2012). The latter approach gives the most robust definition of thrust and drag, but is not generally applicable to measurements on swimming fish because it requires quantitative estimates of fluctuating force distributions along the body.

Many approaches have been used to measure, estimate or calculate the hydrodynamic forces. With an inverse-dynamics approach, resultant forces and torques on the body have been calculated from swimming kinematics of larval zebrafish (2D: Fig. 3C; Van Leeuwen et al., 2015b; 3D: Voesenek et al., 2016). Particle image velocimetry (PIV; see Glossary) techniques have been used to quantify flow fields around swimming fish larvae (e.g. Müller et al., 2008), allowing the estimation of resultant hydrodynamic forces (Unal et al., 1997; Drucker and Lauder, 1999; Dabiri, 2005). In addition, velocity fields obtained with PIV have been used to estimate pressure fields in a horizontal plane around swimming fish (Dabiri et al., 2013). From the velocity gradient near the body, the shear-stress distribution can be calculated. Therefore, in principle, it is possible to calculate the force distribution on the skin from a velocity field around the fish. In practice, it is difficult to quantify this near-body velocity field with PIV [or with particle tracking velocimetry (PTV; see Glossary)]. Because the flow field around a swimming fish is fundamentally 3D (e.g. Fig. 4), 3D PIV/PTV techniques (e.g. Elsinga et al., 2006) are required. These techniques are expensive and still have a relatively low spatial resolution, leading to inaccurate estimations of pressure

Journal of Experimental Biology (2018) 221, jeb149583. doi:10.1242/jeb.149583

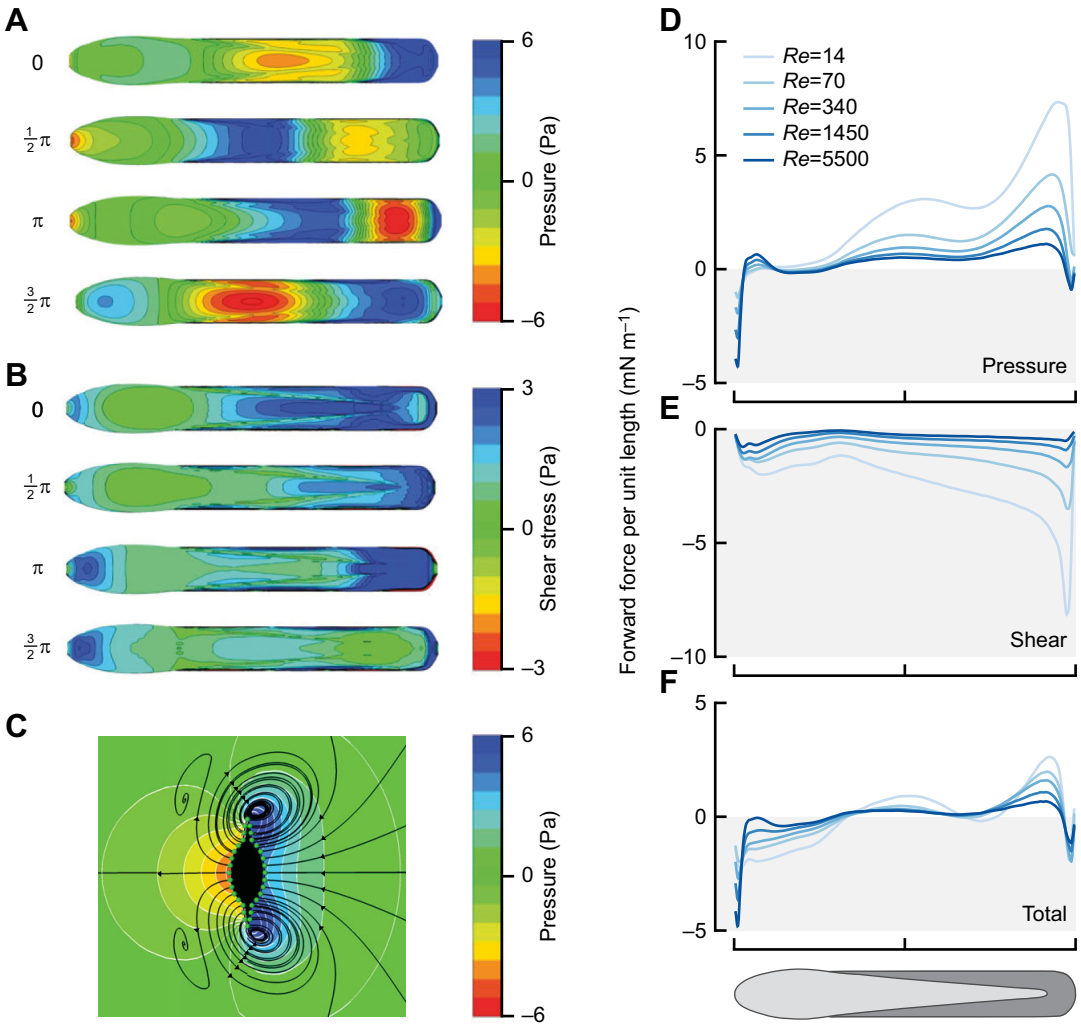

Fig. 4. Predicted hydrodynamic force generation by a simplified zebrafish larva at different Reynolds numbers (*Re*). These data are from three-dimensional (3D) computational fluid dynamics of a simplified model of a zebrafish larva with dorsoventral symmetry, for which the travelling body waves were prescribed, and the changing body position and yaw were computed from fluid-dynamic forces. (A,B) Surface pressure (A) and shear stress (B) on the left side of the fish at four time instants throughout the cycle; *Re*=340. (C) In-plane streamlines (lines) and pressure (contours) in a typical transversal cross-section. (D–F) Cycle-averaged forward component of the pressure force (D), shear force (E) and total force (F) per unit length along the body at different *Re*. Shear forces contribute almost exclusively to drag, and their relative importance with respect to pressure forces increases with decreasing *Re*. Adapted from Li et al. (2016).

and shear-stress distributions on the skin. This makes it difficult to obtain reliable force distributions from PIV or PTV.

Force distributions on the fish have been calculated using fluid-dynamic models. In the inertial flow regime, Lighthill's elongated body theory (Lighthill, 1960, 1971) has been used extensively. However, this model is not applicable to the intermediate flow regime because it models only inertial forces and ignores friction (Borazjani and Sotiropoulos, 2009). Simplified fluid-dynamic models have been proposed (Jordan, 1996; Chen et al., 2011) where the force on every segment of the body is calculated based only on the motion of that segment. However, this does not take into account spatial and temporal interactions between segments. Especially for large-amplitude body motion, these assumptions might not hold (Van Leeuwen et al., 2015b). More advanced models have been applied by, for example, Eloy (2013), who combined different empirical models to achieve more accurate fluid-dynamic forces. Finally, the full Navier–Stokes equations describing fluid dynamics have been approximated numerically using computational fluid dynamics (CFD) techniques for swimming animals, for example tadpoles (Liu et al., 1997), a modelled eel-like swimmer (Kern and Koumoutsakos, 2006) and zebrafish larvae (Li et al., 2012). This approach has the advantage of capturing the complete fluid dynamics, and may provide accurate force distributions on the skin in the intermediate flow regime. In the inertial flow regime, where turbulence may be important, large-scale differences exist within the flow – from the smallest turbulent vortices to the much larger wake vortices – which makes accurate numerical flow computations challenging with the current technology. In contrast, the scale differences are much smaller in the intermediate flow regime, allowing all scales of the flow to be resolved at achievable computational cost. The calculated flow fields can be validated with flow measurements, for example with planar PIV (Li et al., 2012). We expect that, in the future, a combination of measured kinematics, flow fields and validated CFD will allow accurate estimation of force distributions for arbitrary 3D motion.

Such a CFD approach can help us to answer why small fish larvae show high body curvatures along a large range of the body. For fish swimming in the intermediate flow regime, the relatively high

Journal of Experimental Biology (2018) 221, jeb149583. doi:10.1242/jeb.149583

viscous forces result in three negative effects on swimming performance: (1) relatively high skin friction results in a relatively high body drag (Fig. 4; Li et al., 2012), (2) thrust is more costly to produce (Najafi and Golestanian, 2004), and (3) the increased amplitudes of the body undulations, necessary to compensate for the relatively high body drag, themselves further increase drag (Van Leeuwen et al., 2015b). Fig. 4D–F shows the contribution of pressure and shear (friction) forces to the thrust and drag for a modelled zebrafish larvae swimming at different *Re*, calculated using CFD (Li et al., 2016). The shear forces contribute almost exclusively to drag (Fig. 4E), and their relative importance increases with decreasing *Re*. For the lowest *Re* values (<100), a particularly high contribution to friction drag is present in the posterior region, where relatively strong velocity gradients occur near the skin. Most likely to compensate for the strong friction effects upon drag, the larval fish generates thrust by producing high-amplitude, high-frequency body motions (Verhagen, 2004; Müller and Van Leeuwen, 2004; Van Leeuwen et al., 2015b). This results in a pressure difference across the undulating body (Fig. 4D; Li et al., 2016), with large contributions of dorsal- and ventral-edge vortices created at the sharp edges of the finfold (Fig. 4C). The highest contribution to thrust is present in the posterior region.

An intriguing experiment with adult African lungfish (*Protopterus annectens*; *l*=510–590 mm, two orders larger than larval fish) demonstrated the importance of the *Re* regime for drag and thrust production (Horner and Jayne, 2008). The viscosity of the surrounding fluid was increased up to three orders of magnitude by adding a polymer to the water, pushing the Reynolds number of the swimming adult fish into the intermediate flow regime. The lungfish swam with increased muscle activity and body curvature in the mid and anterior regions of its trunk, with bending amplitudes (relative to *l*) approximating those of fish larvae swimming in plain water. The higher drag at a given swimming speed in the more viscous regime presumably required an increased bending effort to generate a similarly higher thrust – the adult lungfish seem to deal with the increased viscous forces similarly to the much smaller larvae. Note that the tail beat frequency did not reach values similar to larval fish because the much larger body inertia of the lungfish presumably prevented this.

The dimensionless Strouhal number (*St*; see Glossary) is an important quantity relating tail beat characteristics and forward velocity and is defined as (Triantafyllou et al., 1993):

$$St = \frac{fA}{\bar{v}}\ , \qquad (2)$$

where f is tail beat frequency and A is peak-to-peak tail amplitude. The Strouhal number gives an indication of the wake topology; assuming that vortices are shed at the extremes of the lateral tail motion, they are laterally spaced at a distance A and longitudinally at a distance $\bar{v}(2f)^{-1}$ (Fig. 5A). The Strouhal number of a swimming fish also defines the ratio between oscillatory flow velocities induced by the beating tail (that scale with fA) and translatory flow velocities (associated with $\bar{v}$). Drag on an animal scales approximately with $\bar{v}^2$, whereas thrust scales approximately with $(fA)^2$. A poorly streamlined animal generates relatively high body drag at a given $\bar{v}$ and, thus, to swim periodically, it needs to generate an equally high thrust force, which is achieved by increasing fA. For this reason, poorly streamlined animals need to swim at a relatively high *St* to produce enough thrust to counter drag, such as crocodiles swimming at *St*=0.78 (Eloy, 2012, based on data of Seebacher et al., 2003). For a similar reason, animals that are 'streamlined' but operate at low *Re* need also to swim at high *St* (e.g. the lungfish described above) because the relatively strong viscous effects similarly result in increased body drag, which consequently requires an equal increase in thrust production. Owing to this dependency on the friction forces, *St* varies with *Re* in the intermediate flow regime (Fig. 5A; Kayan et al., 1978; Borazjani and Sotiropoulos, 2009; Van Leeuwen et al., 2015b).

Energetics

Energy efficiency is important for fish in general, and especially for larvae. Young larvae have a limited amount of energy in their yolk and are not yet able to feed. Because the 'primary goal' of the larva is to reach the reproductive adult stage and produce offspring, they need to use as much of this yolk for growth and development as possible. Because swimming activity can contribute up to 80% of the total metabolism [for larval cod (Ruzicka and Gallager, 2006)], saving energy on locomotion can have a large impact on the total energy budget. Therefore, it is useful to define a measure of swimming energetics for comparison between species and between developmental stages.

Based on the efficiency of thrust production of an oscillating foil in the inertial flow regime, Triantafyllou and colleagues (1993)

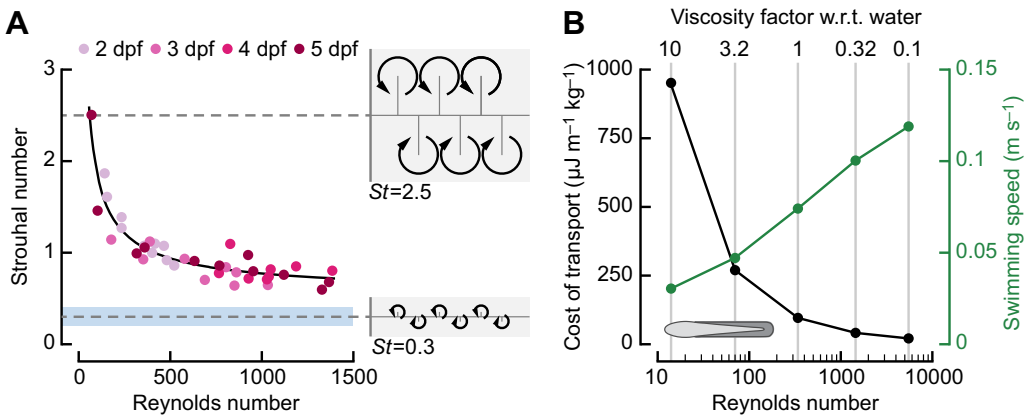

Fig. 5. Effects of Reynolds number (*Re*) on the Strouhal number (*St*) and cost of transport (CoT). (A) *St* versus *Re* for zebrafish (*Danio rerio*) larvae of four age classes (colours). Data from Van Leeuwen et al. (2015a,b). The blue region is the suggested optimal *St* range of 0.2–0.4 from Taylor et al. (2003). Indicated on the right, connected to the dashed lines, are theoretical wake patterns for *St*=0.3 and 2.5. (B) CoT (black) and swimming speed (green) versus *Re* of a simplified computational model of a zebrafish larva swimming in fluids with different viscosities, using the same body curvature fluctuations. Despite the increase in swimming speed with decreasing viscosity, CoT reduces with *Re*. Data from Li et al. (2016). w.r.t., with respect to.

proposed that optimal efficiency is achieved for *St* values of 0.25–0.35, where the vortices shed by the fish are optimally reused for thrust production. For the inertial regime, most examined flying and swimming animals have been found to operate in an *St* range of 0.2–0.4 (Taylor et al., 2003). In contrast, within the intermediate regime, animals tend to operate at higher *St* than the optimal range for inertia-dominated flows (Fig. 5A; Eloy, 2012; Van Leeuwen et al., 2015b). To produce sufficient thrust to overcome the relatively high (viscous) drag at a given swimming speed (see Fluid dynamics section, above), animals swimming in the intermediate *Re* regime may need to operate at relatively high *St*. Further research is required to elucidate the link between *St* value and energy use for the intermediate flow regime.

Another measure often used in the analysis of swimming energetics is the Froude efficiency (η) (Lighthill, 1960), defined as:

$$\eta = \frac{\bar{P}_{\text{output}}}{\bar{P}_{\text{input}}} = \frac{\bar{T}\bar{v}}{\bar{P}_{\text{input}}} = \frac{\bar{D}\bar{v}}{\bar{P}_{\text{input}}}\ , \tag{3}$$

where $\bar{P}_{\text{input}}$ and $\bar{P}_{\text{output}}$ are the cycle-averaged input and output power, respectively. The output power consists of the product of cycle-averaged swimming speed ($\bar{v}$) and magnitude of thrust ($\bar{T}$) or drag ($\bar{D}$), which are equal during cyclic swimming. However, as mentioned above, unambiguously separating drag and thrust requires extensive computational effort, which is not feasible in many cases. But, most importantly, η does not relate to absolute power consumption, a quantity crucial to the fish. To illustrate, consider a high-drag fish and a low-drag fish swimming at the same speed with identical η. The high-drag fish has a higher output power ($\bar{D}\bar{v}$) than the low-drag fish, and therefore requires a higher input power, despite having the same η. In agreement with Schultz and Webb (2002), these reasons make Froude efficiency unsuitable as a measure of energetics for whole-body swimmers such as fish larvae.

Instead, a measure of swimming energetics during cruising should give a direct indication of swimming-related power consumption (Schultz and Webb, 2002). Cost of transport (CoT) (Schmidt-Nielsen, 1972) is defined as a locomotion-related energy consumption per unit distance and unit mass:

$$\text{CoT} = \frac{E_{\text{input}}}{dm} = \frac{\bar{P}_{\text{input}}}{\bar{v}m}\ , \tag{4}$$

where E_{input} is input energy required for locomotion, d is covered distance and m is the mass of the fish. The CoT is directly relevant to the energetics of the animal – minimising CoT at a particular swimming speed is identical to minimising power (and therefore energy) consumption. Furthermore, determining CoT is not burdened by the difficulties associated with separating thrust and drag. The CoT is relevant for cruising fish, swimming either (approximately) cyclically or by burst-and-coast. It is less suitable for motions where maximum acceleration and short response times are paramount, such as fast starts. Here, an efficiency-like quantity could be used, taking for example the ratio of the final kinetic energy to the total invested energy.

To calculate CoT, multiple definitions of the input power are possible, either derived only from the fluid and body dynamics or, better, taking into account all sources of increased energy expenditure due to locomotion, including for example muscles and circulation. The first, which ignores the conversion losses of metabolic energy into muscle work, can be calculated from CFD results (e.g. Li et al., 2012), whereas the latter can be determined from, for example, respiration flow-tunnel experiments (e.g. Madan Mohan Rao, 1971; Palstra et al., 2008). These experiments are, however, challenging for small larval fish because they tend to swim in the (low speed) boundary layer or even adhere to the bottom. Therefore, to measure the swimming speed in a flow tunnel accurately, the flow profile of the tunnel and the position of the larva within it need to be quantified. Note that the locomotion-related energy consumption should be extracted from the respirometry-derived total energy consumption by correcting for the basal metabolic rate.

The body and fluid-dynamic components of the CoT give insight into the energy expended into the flow, but the quantity directly relevant to the fish is the muscle input power – the power that is actually consumed for swimming. Because the muscle efficiency depends on shortening rate and frequency (Curtin and Woledge, 1993), which in turn depend on the motion of the fish, optimal swimming for minimal muscle power presumably needs to compromise between efficient fluid dynamics and optimal muscle shortening rates. Therefore, the optimal swimming motion that minimises fluid-dynamic power will in general not minimise muscle power. Hence, depending on the type of analysis, care should be taken to clearly define the CoT.

Li et al. (2012) studied the effect of swimming speed on (body and fluid-dynamic) power consumption for a simplified model of a zebrafish by varying curvature amplitude. This showed that CoT increases with swimming speed, presumably caused by an increase in drag. Fig. 5B shows the swimming speed and (body and fluid-dynamic) CoT for a similar model larva swimming at different viscosities with identical body-curvature fluctuations (Li et al., 2016). Owing to a reduction in viscous forces at a higher *Re*, thrust and drag are balanced at a higher swimming speed. Despite this higher speed, CoT is lower at a higher *Re*: the hydrodynamic regime influences CoT strongly.

Fish larvae can actively change their CoT by selecting the speed at which they swim: a lower speed tends to result in a lower CoT (Li et al., 2012). However, constraints often exist on the time spent to cover a distance. The larva needs to compromise between energy consumption and travel time. For example, for a foraging larva, the amount of consumed food tends to increase with the average swimming speed, as does the CoT (i.e. power consumption). In this case, the optimal swimming speed might be the one that leads to the highest net energy gain (energy gained from the food minus the costs for catching and processing), balancing between food intake and energy spent on locomotion (Ware, 1975).

Muscles

Fish larvae power swimming with their axial muscle system. The varying demands on the muscular system throughout development require continuous molecular changes and spatial rearrangement of muscle fibres, as well as changes in the neural pattern generators that orchestrate the spatiotemporal muscle activation. Given the size and scope of this Review, we do not intend to provide a broad overview of the regulation of muscle development and the molecular changes that occur during the larval phase. Instead, we highlight selected biomechanical challenges that fish larvae need to cope with and point at evolved solutions.

The trunk muscles in bony fish are arranged in two rostrocaudal series of myomeres, one at each side of the body, that power the lateral bending of the body during swimming (Fig. 6A). It is advantageous if all muscle fibres in the myomeres can usefully contribute to the mechanical work required to bend the body, and thus power swimming (Alexander, 1969; Van Leeuwen et al., 2008). To achieve this, active muscle fibres need to contract at similar strains, which depend on their lateral position and

Journal of Experimental Biology (2018) 221, jeb149583. doi:10.1242/jeb.149583

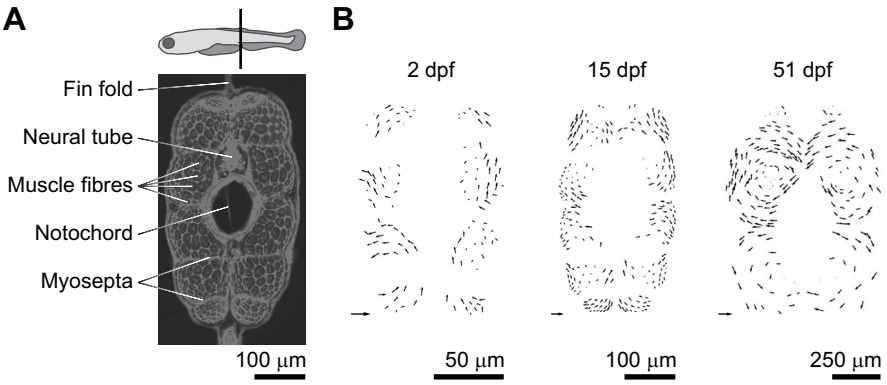

Fig. 6. Muscle-fibre reorientation during development of zebrafish. (A) Cross-section of the trunk muscle of a 15-dpf zebrafish larva. The diagram at the top indicates the location of the slice, at the anus. Note that only a subset of muscle fibres and myosepta has been labelled. (B) Reorientation of muscle fibres over development of a larval zebrafish, for 2, 15 and 51 dpf. The vectors indicate muscle-fibre directions. Each vector is of unit length (indicated by the reference vector at the bottom left) in 3D. Hence, from the length of each projected vector, the angle with the projection plane can be deduced. Adapted from Van Leeuwen et al. (2008), who used data for 51 dpf larvae from Mos and Van der Stelt (1982).

orientation. Van Leeuwen and colleagues (2008) showed that, in zebrafish, the internal arrangement of the muscle fibres changes over development – they initially have an approximately longitudinal orientation and rearrange over ontogeny to form near-helical muscle-fibre trajectories (Fig. 6B). Van Leeuwen et al. (2008) suggested that the fibre reorientation results in reduced variation of the longitudinal muscle-fibre strain over the muscle volume, allowing all muscle fibres to contribute effectively to work production. Although it is still unclear by which mechanism the muscle fibres rearrange, it was shown that larvae that cannot activate their trunk muscles undergo a much-reduced reorientation (Van der Meulen et al., 2005). This suggests that the muscle-fibre forces and the deformation of the trunk are essential for the muscle-fibre rearrangement.

Small fish larvae reach relatively high swimming speeds by beating their tails at high frequencies with large amplitude. Within hours after hatching at 2 dpf, larval zebrafish can swim with tail beat frequencies of ∼80 Hz, and 1 or 2 days later even at 90–100 Hz (Müller and Van Leeuwen, 2004; Van Leeuwen et al., 2015b), allowing them to reach swimming speeds of ∼65 body lengths s^{-1}. To generate these fast motions, the muscle system needs to produce high strain rates, and activate and deactivate at a high frequency. To meet these requirements, bony fish larvae have evolved ‘specialised’ very fast larval (embryonic) muscle-fibre types that are distinct from the slow (red), intermediate and fast (white) fibres found in juvenile and adult zebrafish (Buss and Drapeau, 2000). What makes these larval muscle fibres so very fast? They are short [<200 μm in 7 dpf carp larvae (Alami-Durante et al., 1997)], leading to small activation delays along the fibre. High-frequency contractions require fast release and uptake of Ca^{2+} from the sarcoplasmic reticulum (SR). This is made possible by a relatively large membrane surface of the SR and by short diffusion distances within myofibrils with a comparatively small diameter [∼0.3 μm in larval herring (Vieira and Johnston, 1992); ∼1–1.2 μm in adult saithe (Patterson and Goldspink, 1976)]. Furthermore, different isotypes of the Ca^{2+}-binding protein parvalbumin are expressed over development (Focant et al., 1992; Huriaux et al., 1996), suggesting specific adaptations to the demands on fast Ca^{2+} release and uptake. In addition, fish larvae have distinct isoforms of myosin heavy chain and myosin light chain proteins compared with those of juveniles and adults (Scapolo et al., 1988; Crockford and Johnston, 1993; Huriaux et al., 1999; Veggetti et al., 1993), which is suggested to correspond to the extreme demands in larvae. Early fish larvae have been observed to have high mitochondrial densities in the muscle (Vieira and Johnston, 1992; Brooks et al., 1995). This, together with the short diffusion distances, suggests that small larvae always swim almost entirely aerobically with their very fast muscle (El-Fiky et al., 1987; Wieser, 1995). As the larvae grow, tail beat frequencies are decreased owing to the increasing body inertia. At this stage, slower muscle-fibre types appear, suitable for cruising aerobically with higher efficiency than the very fast muscles (Mascarello et al., 1995).

The muscle system needs specific activation patterns to perform effective swimming motion. Muscle activation patterns during swimming are often measured with electromyography (EMG) in adult fish (e.g. Blight, 1976; Van Leeuwen et al., 1990; Horner and Jayne, 2008). For smaller larval fish, this technique is difficult without strongly disrupting swimming behaviour. Muscle activation patterns were measured in so-called fictive swimming, where a paralysed fish is stimulated to swim and an EMG signal is recorded at the muscles (Buss and Drapeau, 2002). These investigations showed that muscle activation patterns in larval zebrafish are similar to those of the adult fish, with alternating left–right activation of the muscle with a rostrocaudal delay. More recently, a method was proposed to measure muscle activity on a fixed, but non-anaesthetised, zebrafish larva (Cho et al., 2015). However, as far as we are aware, no muscle-activation-pattern measurements have been performed on free-swimming larval fish, limiting our knowledge on the locomotory control in fish larvae.

To drive the very fast muscle system, the neural motor system should be up to the task of generating very fast activation patterns. The motoneurons in the spinal cord of the larval zebrafish that innervate the muscles are arranged in left and right dorsoventral columns (McLean et al., 2007; Fetcho and McLean, 2010). The fastest primary motoneurons lie dorsally and activate high-power, high-frequency motions, whereas the slowest motoneurons lie ventrally and activate finely controlled low-frequency motions. The fastest motoneurons develop first; the slowest motoneurons develop last. Thus, the functionally different motoneurons are spatially segregated and their appearance is shifted in time. McLean and colleagues (2007) suggested that the activation of the motoneurons takes place according to the size principle (Henneman et al., 1965) – the dorsal motoneurons are larger than the ventral ones and more difficult to recruit. In the hindbrain, very large so-called Mauthner (and homologous) neurons are already present in just-hatched larvae. Their axons run along the entire spinal cord and innervate motoneurons. These neurons drive the fast starts by initiating an almost instantaneous activation along one side of the trunk (see Escaping predators section, below). The early presence of the Mauthner neurons and their homologues, and the fastest motoneurons, support fast high-frequency motions from the day of hatching in the larval zebrafish, but fine control is still lacking owing to the absence of functional slower motoneurons, which are still developing. This results in fast but ‘visually chaotic’ swimming motions of 2-dpf larvae, which seem hard to predict and might still be effective for predator avoidance. Later in development, the

response to threats becomes more refined (see also Escaping predators section, below).

Cruising and dispersal

An obvious reason to swim is to cover distance for migration and dispersal: many fish larvae disperse early in development, travelling long distances (e.g. Sancho et al., 1997; Dudley et al., 2000). For late-stage reef-fish larvae, active swimming might affect dispersion at a magnitude comparable to that of oceanic currents (Fisher, 2005; Huebert and Sponaugle, 2009). These late-stage larvae are relatively large (15–30 mm) and swim at relatively high speeds [~0.2–0.6 m s^{-1}, ~10–20 body lengths s^{-1} (Fisher, 2005)], and so their *Re* values (3300–20,000) are well within the inertial regime. The resulting low CoT allows them to disperse over longer distances, and their relatively high swimming speed allows them to achieve this within a suitable time window. Even larvae of non-migrating species often need to cruise. Larvae foraging in habitats of low food abundance need to swim relatively long distances to find prey. In addition, in the presence of a prevailing current, larvae need to swim for prolonged periods to remain in their current habitat, unless they have an organ to attach themselves to the substrate (Able et al., 1984; Pottin et al., 2010).

Virtually all bony-fish larvae have a functional finfold when they hatch (Kendall et al., 1984). To what extent could such a finfold be useful for swimming in the intermediate flow regime? As explained above (see Fig. 4), fish larvae swimming in this regime need to produce high thrust to compensate for high drag. To this end, fish larvae adopt an anguilliform swimming style, with a large region along the body that curves substantially and produces thrust. Using CFD, Li and colleagues (2016) showed that production of thrust is enhanced by edge vortices emanating from a sharp edge, making a finfold surrounding a large part of the body an effective adaptation to increase thrust. Keeping the body-curvature fluctuations the same, they also computed that a removal of the finfold, except for the caudal fin, leads to a decrease in swimming speed and fluid-dynamic power input, but with almost the same fluid-dynamic CoT. Thus, compared with the finfold-less larval morph, the morph with finfold covers distance within a shorter time with the same fluid-dynamic costs. This might be advantageous during migration and searching for prey, if the higher power can be delivered with the muscular system. These findings might help to explain the omnipresence of the finfold in larval bony fish.

As the larvae grow, inertia becomes more important during swimming. The associated relative drag reduction allows many fish to shift towards a carangiform swimming mode (see Glossary) by reducing the relative curvature amplitude along their bodies (see Body kinematics section; Osse and Van den Boogaart, 2000). This change in swimming style correlates with development of a separate caudal fin in many species (Osse and Van den Boogaart, 1995). In some species, development of the caudal fin occurs before that of other unpaired fins, presumably because it has the largest contribution to thrust production [black rockfish (Omori et al., 1996), yellow-fin mullet (Kingsford and Tricklebank, 1991)].

Escaping predators

Predation is an important cause of mortality in fish larvae (Sogard, 1997). Hence, the chances of survival will increase with increasing ability to escape predators. Larval fish generally attempt to escape predators by performing a ‘C-start’, during which they curl their body into a C-shape, with little movement of the CoM (stage 1, or preparatory stroke), and then uncurl to generate high thrust, and therefore high accelerations of their CoM [stage 2, or propulsive stroke (Müller et al., 2008)]. This motion is often followed by a high-amplitude, high-frequency swimming bout (Müller and Van Leeuwen, 2004). Fig. 7A shows an example of a 3D kinematic analysis of a fast-starting zebrafish larva (data in Dataset 1), illustrating the strong body curvature at the end of the C-phase, the subsequent push-off phase with a rapid increase in CoM velocity, and the 3D nature of the motion. Initiation of the C-start requires fast unilateral activation of the axial muscles [e.g. for adult bluegill sunfish (Jayne and Lauder, 1993)]. Such manoeuvres require concerted actions of the complete locomotory system: the sensory-motor system needs to detect threats reliably, and initiate and control the escape; the muscular system should produce enough force and power at short activation times; and the external morphology needs to support effective hydrodynamic thrust production to maximise acceleration.

Producing high accelerations and velocities

During the preparatory stroke, zebrafish larvae produce a jet flow into the C-form (Fig. 7B; Li et al., 2014; Müller et al., 2008). The resulting pressure distribution on the body mainly produces a torque that rotates the larva (Li et al., 2012). In the following propulsive stroke, the jet is reoriented along the body (Fig. 7B), where the pressure distribution propels the fish forward and provides a torque that counteracts the angular velocity produced in the preparatory stroke. The relatively high thrust results in high accelerations; for zebrafish, up to 28 **g** (Müller and Van Leeuwen, 2004). CFD simulations indicate that the typical motions of a C-start in larval fish tend to maximise escape distance (Gazzola et al., 2012). After the propulsive phase, larvae use large-amplitude high-frequency motion, up to ~100 Hz [zebrafish (Müller and Van Leeuwen, 2004; Van Leeuwen et al., 2015b)]. Larval fish increase their fast-start performance over development, decreasing the time spent performing a start and increasing the distance within that time, which is suggested to be associated with an increase in *Re* [Chinook salmon (Hale, 1996)].

The high-frequency body undulations require the muscle system to operate at the same high frequencies and produce relatively high forces and power within a short time (<5 ms) to push off against the water with the tail. These short high-amplitude contractions lead to high strain rates, and put high demands on the activation and deactivation systems. This conflicts with the requirement to produce high force: superfast muscle required for high-frequency swimming tends to produce low tensile stresses at low efficiency (Rome et al., 1999). However, because the larvae are small, scaling works in their favour: the produced force is proportional to the muscle physiological cross-section, which scales with l^2, whereas body mass is approximately proportional to the volume, which scales with l^3. The favourable ratio of muscle cross-section to body inertia allows larvae to produce sufficient muscle force to power strong accelerations. Furthermore, fish larvae might employ an elastic mechanism to support swimming at high frequencies (Müller and Van Leeuwen, 2004). For example, larval carp have smaller, stiffer isoforms of titin than adults, suggested to contribute to an increased muscle and body stiffness and possibly elastic energy storage (Spierts, 2001). As fish larvae grow, the required hydrodynamic power for escaping increases but it is compensated by a decrease in the required muscle shortening velocity and an increase in muscle mass, leading to an increase in total muscle force and power [carp (Wakeling et al., 1999)].

Timing and controlling the escape

When attacked by a slow-moving predator, as is often the case for suction-feeding predators (Webb, 1984), fish larvae may reach

Journal of Experimental Biology (2018) 221, jeb149583. doi:10.1242/jeb.149583

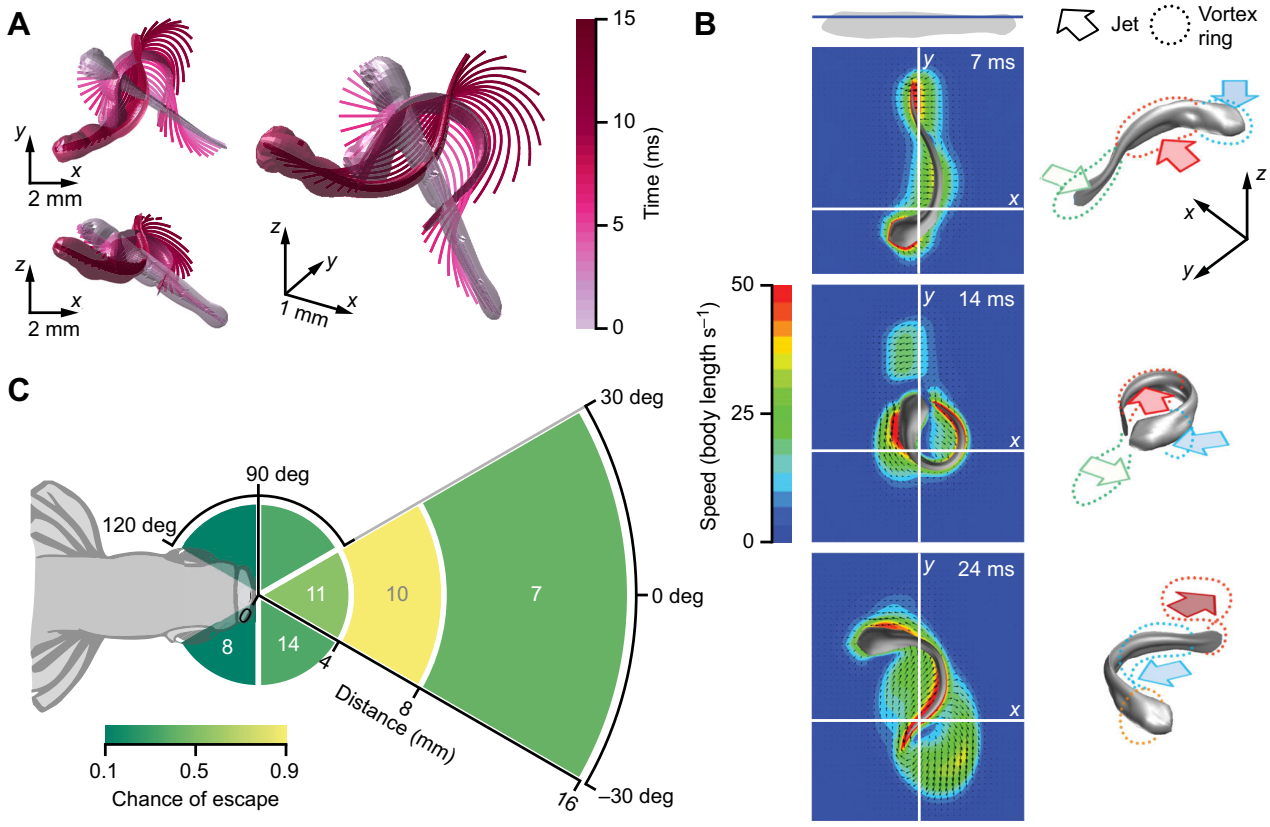

Fig. 7. Escape responses by larval fish. (A) Fast-start escape response by a 3-dpf zebrafish larva (top view, side view and 3D view) automatically tracked from three synchronised high-speed video cameras at 2000 frames s^{-1} using the setup and method described in Voesenek et al. (2016). Fish midlines are indicated in 3D with lines coloured by time. In all views, three 3D renders are shown: at the start of the escape, at the end of stage 1 and at the end of stage 2. Based on unpublished data by C.J.V., R. P. M. Pieters and J.L.v.L. (B) Contours of velocity magnitude and velocity vectors around a zebrafish larva performing a C-start, simulated with computational fluid dynamics (CFD), along with sketches of the flow illustrating the evolution of jets and vortex rings, at different time instants. The contour plots are shown in the *x*–*y* plane, at the height indicated by the blue line over the sketch of the zebrafish. In the sketches at the right, jets (arrows) and vortex rings (dotted lines) with the same colours over multiple time instants indicate that they are the same structure. Adapted from Li et al. (2014). (C) Timing of escape responses is important for survival. The probability of escape depends on distance from the predator's mouth, and the angle with respect to the predator's heading. In the figure, the sketch of the fish head represents the predator; the escape probability is indicated by colour, binned by angle and distance; inside each bin is the number of samples. Adapted from Stewart et al. (2013).

higher speeds than the predator. In these cases, predator detection rather than locomotor performance has been suggested to be the most important determinant of escape success (Nair et al., 2017). Prey escape success in zebrafish larvae is highest when they respond at an intermediate distance (4–8 mm) from the predator (Fig. 7C; Stewart et al., 2013). Larger response distances allow the predator to adjust its intercept course, whereas smaller distances do not give the larvae enough time to escape. This places requirements on the sensing systems, to detect predators sufficiently early, and on the control of the escape, to perform an adequate response.

Flow sensing using the lateral line (see Glossary) plays an important role for predator detection (McHenry et al., 2009). Zebrafish larvae detect the approach of a predator by sensing pressure differences, and escape in the direction away from the fastest flow (Stewart et al., 2014). In Atlantic herring, late-stage larvae make more-sophisticated escape manoeuvres than younger larvae and undergo fewer false alarms (Fuiman, 1993), suggesting that they become better at performing a proportional and well-timed response, presumably owing to learning, and improved sensing and control capabilities.

Fish larvae also use visual cues to detect threats. Zebrafish larvae of 5–6 dpf respond to a growing dark spot (i.e. a looming stimulus) by performing an escape manoeuvre after it has reached a critical size on the retina, suggesting relatively advanced visual processing early in development (Dunn et al., 2016). Herring larvae only show responses to looming stimuli late in development (at 25 mm body length), whereas early larvae do respond to flashing stimuli, indicating that visual processing power increases over development (Batty, 1989). Compared with sound or touch, visual responses result in more escape trajectories directed away from the stimulus. Hence, it is likely that improvements in the sensory systems allow older fish larvae to escape predators more effectively.

Fast reaction times place requirements on the neural control of escape manoeuvres and sensors to detect approaching predators. The fast-start response to stimuli is controlled mainly by the Mauthner neurons and their homologues (Wilson, 1959; Foreman and Eaton, 1993). A group of three reticulospinal neurons – the Mauthner cell, MiD2cm and MiD3cm – initiates escape manoeuvres in zebrafish larvae: the Mauthner cell is involved in responding to tail-directed stimuli, whereas the two other neurons respond to head-directed stimuli (Liu and Fetcho, 1999). This system develops early in zebrafish: larvae show a strong swimming response to touch stimuli after 2 days of development (Eaton and Farley, 1973), allowing them to respond to threats immediately after

Journal of Experimental Biology (2018) 221, jeb149583. doi:10.1242/jeb.149583

hatching. The response time to visual stimuli is often much larger than that of acoustic stimuli, and delays in both decrease throughout development [red drum larvae (Fuiman et al., 1999)].

Following an optimal escape trajectory requires precise control of muscle activation patterns. In adult goldfish, the escape trajectory is controlled by the relative magnitude of ipsilateral and contralateral muscle contraction, and by the delay between them (Foreman and Eaton, 1993). Furthermore, fish larvae actively regulate the elevation angle of their fast starts, likely by separate activation of hypaxial and epaxial muscle [zebrafish (Nair et al., 2015)], and presumably also by using their medial and paired fins. During a strong C-start, an escaping larva can intercept its own wake, which causes a deflection of the escape path of more than 5 deg (Li et al., 2014). For precise control over the final heading of the escape trajectory, this should be taken into account by the neural control system.

Hunting and feeding

The vast majority of hatched fish larvae die before they reach the juvenile stage, often owing to starvation (Hjort, 1914; Houde, 2002). As soon as larvae exhaust their yolk, they need to hunt prey to meet their energy requirements. Limited energy supply arising from ineffective feeding can cause starvation; in a less extreme case, it can limit the growth rate of the larva (Lee et al., 2010). The resulting smaller size might negatively affect survival owing to increased predation of smaller larvae (Peterson and Wroblewski, 1984). To gather the required food, nearly all teleost fish larvae are pelagic suction feeders preying on zooplankton after they exhaust their yolk sac (Hunter, 1980; Drost, 1987). Suction feeding places requirements on the developing fish: it needs to be able to detect prey, approach it while aiming the mouth, create an accurately timed suction flow, and subsequently swallow and digest the prey (Osse, 1989). The hydrodynamics of suction feeding depends on the Reynolds number. Feeding under relatively viscous conditions generally seems less successful because the prey can more easily escape the suction, requiring smaller forces than in a less viscous flow regime (China and Holzman, 2014). For this reason, larger fish can catch more prey and hence survive longer.

The locomotory system supports suction feeding by allowing the fish to control and time its prey approach for effective capture (Van Leeuwen, 1984). During undulatory swimming, the head oscillates with respect to the path of the CoM (Van Leeuwen et al., 2015b). This makes a precise approach of the feeding apparatus towards the prey difficult, especially without creating large flow disturbances that might be sensed by the prey. The fish require specific adaptations to achieve this, either another means of propulsion (e.g. pectoral fins) or specific control patterns that limit head motion and hydrodynamic disturbances [e.g. a J-turn (Bianco et al., 2011)].

Pectoral fin movement to brake and manoeuvre during suction feeding has been observed in adult (Higham, 2007) and juvenile (Lankheet et al., 2016) fish. Pectoral fins have been suggested to play a respiratory function in larval zebrafish, rather than a locomotory one (Green et al., 2011; Hale, 2014), because genetic elimination of the pectoral fins did not seem to influence slow-swimming performance. However, during feeding, they might play an important role in aligning the head through control of the pitch and yaw angles, as well as contributing to forward acceleration and deceleration. Fig. 8A depicts a carp larvae performing a feeding strike (Drost, 1987). It beats the pectoral fins to approach the prey, adducts them against the body and then brakes by flapping them forward. Zebrafish larvae beat their pectoral fins to align themselves before a strike, perform an S-start to accelerate and finally brake

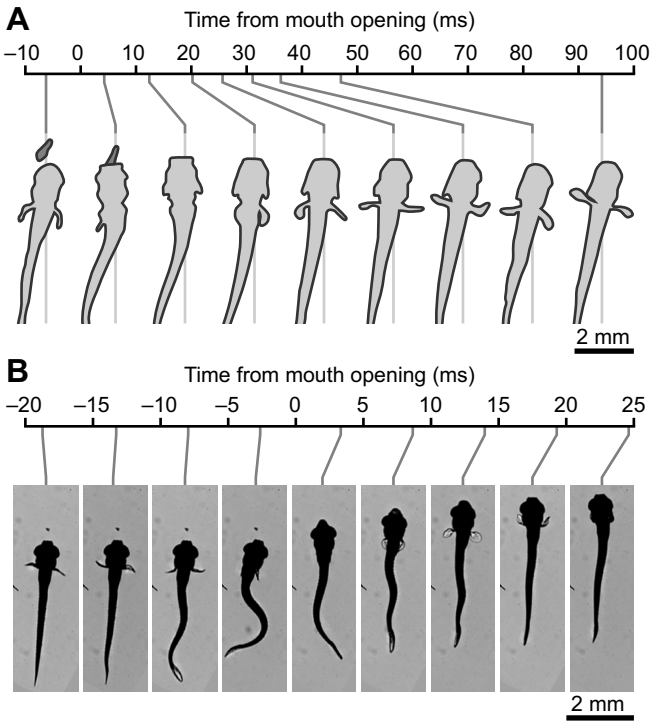

Fig. 8. Pectoral fin use during feeding of carp and zebrafish larvae. (A) Traces from high-speed-video frames of a 6.5-mm carp (*Cyprinus carpio*; pale grey) larva while sucking prey (*Artemia*; dark grey). Redrawn from Drost (1987). (B) High-speed video frames of a 5-dpf zebrafish larva performing a feeding strike on a piece of debris. Based on unpublished data by C.J.V., R. P. M. Pieters and J.L.v.L. For both panels, time is relative to the moment of mouth opening, and each drawing/frame connects to the associated point on the time axis.

using forward motion of the pectoral fins (Fig. 8B). The S-start produces much lower yaw angles of the head than the C-start, allowing for an accurate alignment of the head.

Newborn juvenile guppies (*Girardinus metallicus*) have a partly 'innate' feeding behaviour, but more advanced eye–fin coordination develops rapidly after birth (Lankheet et al., 2016). Early zebrafish larvae (6–8 dpf) have been suggested to have fine motor control during feeding, showing complex bend-to-bend variation in timing and rostrocaudal location of bending (Borla et al., 2002). Prey tracking in zebrafish larvae is visually guided (McElligott and O'Malley, 2005). Because the eye becomes functional only after hatching (which occurs at 2 dpf) [zebrafish (Glass and Dahm, 2004)], rapid development of the visual processing system is required before the first feeding at approximately 5 dpf.

Perspectives

Much work on the swimming of fish has been performed under the assumption of periodic motion, although the majority of swimming behaviour of most (larval) fish is aperiodic. With the exception of fast starts, aperiodic motion has been studied much less. Furthermore, owing to technical limitations, much of the analyses have been done in a single plane, even though swimming motion is often highly 3D. Many open questions remain on the kinematics, fluid dynamics and control of complex 3D manoeuvres often performed by the fish during escape or hunting.

Whereas the fluid dynamics of wakes behind swimming fish has received considerable attention, both experimentally and numerically, the resulting force distributions on the skin have not.

As demonstrated with dedicated CFD solvers (e.g. Li et al., 2016 – see Fluid dynamics section), the fluid dynamics of swimming in the intermediate flow regime and the resulting force distributions can be well modelled using CFD techniques, because the lack of turbulence allows all relevant scales of the flow to be resolved accurately. The advent of open-source fluid-dynamic solvers [e.g. OpenFOAM (Jasak et al., 2007)] make this possible at low cost with comparatively limited programming effort. There are interesting opportunities to numerically investigate force, torque and power production, and 3D manoeuvring, and how these correlate with shifts in the fluid-dynamic regime.

The development and restructuring of the axial muscle of larvae have been investigated in previous studies, but research on the physiological properties and activation patterns of the larval muscle system is relatively limited. Larval fish have adapted to the required high-frequency contractions with specific larval muscle-fibre types, possessing unique properties. Research on these properties could uncover how larval muscle can generate sufficient force at such high frequencies. Furthermore, although many studies have measured muscle activation patterns of swimming adult fish, little is known about these patterns in free-swimming larval fish. These measurements might answer how larvae produce swimming motions with their muscles, how this changes over development and whether muscle control is innate or learned. Owing to the small size of the larvae, both muscle-property and muscle-activation measurements are challenging and will require novel methodologies.

Many studies have addressed different aspects of the biomechanics of larval swimming separately. However, swimming motion is created by a complex interaction between the different components; to understand the system as a whole, the components need to be studied integratively. By combining models and measurements of different systems of the fish, including the neuromuscular system, passive tissues and the fluid dynamics, an *in silico* integrative neuromechanical model of the fish larva can be developed. Although a daunting task, such an approach will allow investigators to study the effect of the variation of a large range of parameters on swimming performance in an unprecedented way, and might therefore answer numerous questions on the locomotory system of larval fish throughout their development.

Acknowledgements
We thank two anonymous reviewers for their insightful comments on the manuscript. We benefited from a longstanding collaboration with U. K. Müller, G. Li, and H. Liu.

Competing interests
The authors declare no competing or financial interests.

Funding
This work was supported by grants from the Netherlands Organization for Scientific Research (Nederlandse Organisatie voor Wetenschappelijk Onderzoek; NWO/ALW-824-15-001 to J.L.v.L. and NWO/VENI-863-14-007 to F.T.M.).

Supplementary information
Supplementary information available online at
http://jeb.biologists.org/lookup/doi/10.1242/jeb.149583.supplemental

References
Able, K. W., Markle, D. F. and Fahay, M. P. (1984). Cyclopteridae: development. In *Ontogeny and Systematics of Fishes* (ed. H. G. Moser, W. J. Richards, D. M. Cohen, M. P. Fahay, J. A. W. Kendall and S. L. Richardson), pp. 428-437. Lawrence, KS: American Society of Ichthyologists and Herpetologists.

Alami-Durante, H., Fauconneau, B., Rouel, M., Escaffre, A. M. and Bergot, P. (1997). Growth and multiplication of white skeletal muscle fibres in carp larvae in relation to somatic growth rate. *J. Fish Biol.* **50**, 1285-1302.

Alexander, R. M. (1969). The orientation of muscle fibres in the myomeres of fishes. *J. Mar. Biol. Assoc. UK* **49**, 263-290.

Anderson, J. D. (2001). *Fundamentals of Aerodynamics*. New York City, NY: McGraw-Hill.

Bainbridge, R. (1960). Speed and stamina in three fish. *J. Exp. Biol.* **37**, 129-153.

Batty, R. S. (1989). Escape responses of herring larvae to visual stimuli. *J. Mar. Biol. Assoc. UK* **69**, 647-654.

Bianco, I. H., Kampff, A. R. and Engert, F. (2011). Prey capture behavior evoked by simple visual stimuli in larval zebrafish. *Front. Syst. Neurosci.* **5**, 1-13.

Blight, A. R. (1976). Undulatory swimming with and without waves of contraction. *Nature* **264**, 352-354.

Borazjani, I. and Sotiropoulos, F. (2009). Numerical investigation of the hydrodynamics of anguilliform swimming in the transitional and inertial flow regimes. *J. Exp. Biol.* **212**, 576-592.

Borla, M. A., Palecek, B., Budick, S. and O'Malley, D. M. (2002). Prey capture by larval zebrafish: evidence for fine axial motor control. *Brain. Behav. Evol.* **60**, 207-229.

Brooks, S., Vieira, V. L. A., Johnston, I. A. and Macheru, P. (1995). Muscle development in larvae of a fast growing tropical freshwater fish, the curimatã-pacú. *J. Fish Biol.* **47**, 1026-1037.

Buss, R. R. and Drapeau, P. (2000). Physiological properties of zebrafish embryonic red and white muscle fibers during early development. *J. Neurophysiol.* **84**, 1545-1557.

Buss, R. R. and Drapeau, P. (2002). Activation of embryonic red and white muscle fibers during fictive swimming in the developing zebrafish. *J. Neurophysiol.* **87**, 1244-1251.

Butail, S. and Paley, D. A. (2012). Three-dimensional reconstruction of the fast-start swimming kinematics of densely schooling fish. *J. R. Soc. Interface* **9**, 77-88.

Chen, J., Friesen, W. O. and Iwasaki, T. (2011). Mechanisms underlying rhythmic locomotion: body-fluid interaction in undulatory swimming. *J. Exp. Biol.* **214**, 561-574.

China, V. and Holzman, R. (2014). Hydrodynamic starvation in first-feeding larval fishes. *Proc. Natl. Acad. Sci. USA* **111**, 8083-8088.

Cho, S.-J., Nam, T.-S., Byun, D., Choi, S.-Y., Kim, M.-K. and Kim, S. (2015). Zebrafish needle EMG: a new tool for high-throughput drug screens. *J. Neurophysiol.* **114**, 2065-2070.

Crockford, T. and Johnston, I. A. (1993). Developmental changes in the composition of myofibrillar proteins in the swimming muscles of Atlantic herring, *Clupea harengus*. *Mar. Biol.* **115**, 15-22.

Curtin, N. A. and Woledge, R. C. (1993). Efficiency of energy conversion during sinusoidal movement of white muscle fibres from the dogfish *Scyliorhinus canicula*. *J. Exp. Biol.* **183**, 137-147.

Dabiri, J. O. (2005). On the estimation of swimming and flying forces from wake measurements. *J. Exp. Biol.* **208**, 3519-3532.

Dabiri, J. O., Bose, S., Gemmell, B. J., Colin, S. P. and Costello, J. H. (2013). An algorithm to estimate unsteady and quasi-steady pressure fields from velocity field measurements. *J. Exp. Biol.* **217**, 331-336.

Drost, M. R. (1987). Relation between aiming and catch success in larval fishes. *Can. J. Fish. Aquat. Sci.* **44**, 304-315.

Drucker, E. G. and Lauder, G. V. (1999). Locomotor forces on a swimming fish: three-dimensional vortex wake dynamics quantified using digital particle image velocimetry. *J. Exp. Biol.* **202**, 2393-2412.

Dudley, B., Tolimieri, N. and Montgomery, J. (2000). Swimming ability of the larvae of some reef fishes from New Zealand waters. *Mar. Freshwater Res.* **51**, 783-787.

Dunn, T. W., Gebhardt, C., Naumann, E. A., Riegler, C., Ahrens, M. B., Engert, F. and Del Bene, F. (2016). Neural circuits underlying visually evoked escapes in larval zebrafish. *Neuron* **89**, 613-628.

Eaton, R. C. and Farley, R. D. (1973). Development of the Mauthner neurons in embryos and larvae of the zebrafish, *Brachydanio rerio*. *Copeia* **1973**, 673-682.

Ehrlich, D. E. and Schoppik, D. (2017). Control of movement initiation underlies the development of balance. *Curr. Biol.* **27**, 334-344.

El-Fiky, N., Hinterleitner, S. and Wieser, W. (1987). Differentiation of swimming muscles and gills, and development of anaerobic power in the larvae of cyprinid fish (Pisces, Teleostei). *Zoomorphology* **107**, 126-132.

Eloy, C. (2012). Optimal Strouhal number for swimming animals. *J. Fluids Struct.* **30**, 205-218.

Eloy, C. (2013). On the best design for undulatory swimming. *J. Fluid Mech.* **717**, 48-89.

Elsinga, G. E., Scarano, F., Wieneke, B. and Van Oudheusden, B. W. (2006). Tomographic particle image velocimetry. *Exp. Fluids* **41**, 933-947.

Fetcho, J. R. and McLean, D. L. (2010). Some principles of organization of spinal neurons underlying locomotion in zebrafish and their implications. *Ann. N. Y. Acad. Sci.* **1198**, 94-104.

Fisher, R. (2005). Swimming speeds of larval coral reef fishes: impacts on self-recruitment and dispersal. *Mar. Ecol. Prog. Ser.* **285**, 223-232.

Focant, B., Huriaux, F., Vandewalle, P., Castelli, M. and Goessens, G. (1992). Myosin, parvalbumin and myofibril expression in barbel (Barbus L.) lateral white muscle during development. *Fish Physiol. Biochem.* **10**, 133-143.

Foreman, M. B. and Eaton, R. C. (1993). The direction change concept for reticulospinal control of goldfish escape. *J. Neurosci.* **13**, 4101-4113.

Fuiman, L. A. (1993). Development of predator evasion in Atlantic herring, *Clupea harengus* L. *Anim. Behav.* **45**, 1101-1116.
Fuiman, L. A. and Webb, P. W. (1988). Ontogeny of routine swimming activity and performance in zebra danios (teleostei: Cyprinidae). *Anim. Behav.* **36**, 250-261.
Fuiman, L. A., Smith, M. E. and Malley, V. N. (1999). Ontogeny of routine swimming speed and startle responses in red drum, with a comparison of responses to acoustic and visual stimuli. *J. Fish Biol.* **55**, 215-226.
Gazzola, M., Van Rees, W. M. and Koumoutsakos, P. (2012). C-start: optimal start of larval fish. *J. Fluid Mech.* **698**, 5-18.
Gisbert, E., Merino, G., Muguet, J. B., Bush, D., Piedrahita, R. H. and Conklin, D. E. (2002). Morphological development and allometric growth patterns in hatchery-reared California halibut larvae. *J. Fish Biol.* **61**, 1217-1229.
Glass, A. S. and Dahm, R. (2004). The zebrafish as a model organism for eye development. *Ophthalmic Res.* **36**, 4-24.
Green, M. H., Ho, R. K. and Hale, M. E. (2011). Movement and function of the pectoral fins of the larval zebrafish (*Danio rerio*) during slow swimming. *J. Exp. Biol.* **214**, 3111-3123.
Hale, M. E. (1996). The development of fast-start performance in fishes: escape kinematics of the chinook salmon (*Oncorhynchus tshawytscha*). *Am. Zool.* **36**, 695-709.
Hale, M. E. (2014). Developmental change in the function of movement systems: transition of the pectoral fins between respiratory and locomotor roles in zebrafish. *Integr. Comp. Biol.* **54**, 238-249.
Henneman, E., Somjen, G. and Carpenter, D. O. (1965). Functional significance of cell size in spinal motoneurons. *J. Neurophysiol.* **28**, 560-580.
Higham, T. E. (2007). Feeding, fins and braking maneuvers: locomotion during prey capture in centrarchid fishes. *J. Exp. Biol.* **210**, 107-117.
Hjort, J. (1914). Fluctuations in the great fisheries of northern Europe, viewed in the light of biological research. *Rapp. P. V. Cons. Perm. Int. Explor. Mer* **20**, 1-228.
Horner, A. M. and Jayne, B. C. (2008). The effects of viscosity on the axial motor pattern and kinematics of the African lungfish (*Protopterus annectens*) during lateral undulatory swimming. *J. Exp. Biol.* **211**, 1612-1622.
Houde, E. D. (2002). Mortality. In *Fishery Science: the Unique Contributions of Early Life Stages* (ed. L. A. Fuiman and R. G. Werner), pp. 64-87. Hoboken, NJ: Blackwell Science Ltd.
Huebert, K. B. and Sponaugle, S. (2009). Observed and simulated swimming trajectories of late-stage coral reef fish larvae off the Florida Keys. *Aquat. Biol.* **7**, 207-216.
Hunter, J. R. (1980). The feeding behavior and ecology of marine fish larvae. In *Fish Behavior and Its Use in the Capture and Culture of Fishes* (ed. J. E. Bardach, J. J. Magnuson, R. C. May and J. M. Reinhart), pp. 287-330. Makati, Philippines: ICLARM.
Huriaux, F., Mélot, F., Vandewalle, P., Collin, S. and Focant, B. (1996). Parvalbumin isotypes in white muscle from three teleost fish: characterization and their expression during development. *Comp. Biochem. Physiol. B Biochem. Mol. Biol.* **113**, 475-484.
Huriaux, F., Vandewalle, P., Baras, E., Legendre, M. and Focant, B. (1999). Myofibrillar proteins in white muscle of the developing African catfish *Heterobranchus longifilis* (Siluriforms, Clariidae). *Fish Physiol. Biochem.* **21**, 287-301.
Jasak, H., Jemcov, A. and Tukovic, Ž. (2007). Openfoam: A C ++ library for complex physics simulations. In *Proc. Int. Work. Coupled Methods Numer. Dyn* (ed. Z. Terze and C. Lacor), pp. 47-66. Zagreb, Croatia: Faculty of Mechanical Engineering and Naval Architecture.
Jayne, B. C. and Lauder, G. V. (1993). Red and white muscle activity and kinematics of the escape response of the bluegill sunfish during swimming. *J. Comp. Physiol. A* **173**, 495-508.
Jordan, C. E. (1996). Coupling internal and external mechanics to predict swimming behavior: a general approach. *Am. Zool.* **36**, 710-722.
Kaji, T., Tanaka, M., Takahashi, Y., Oka, M. and Ishibashi, N. (1996). Preliminary observations on development of pacific bluefin tuna *Thunnus thynnus* (Scombridae) larvae reared in the laboratory, with special reference to the digestive system. *Mar. Freshwater Res.* **47**, 261.
Kavanagh, K. D., Leis, J. M. and Rennis, D. S. (2000). Pomacentridae (damselfishes). In *The Larvae of Indo-Pacific Coastal Fishes: An Identification Guide to Marine Fish Larvae* (ed. J. M. Leis and B. M. Carson-Ewart), pp. 526-535. Leiden, The Netherlands: Brill.
Kayan, V. P., Kozlov, L. F. and Pyatetskii, V. E. (1978). Kinematic characteristics of the swimming of certain aquatic animals. *Fluid Dyn.* **13**, 641-646.
Kendall, A. W., Jr, Ahlstrom, E. H. and Mose, H. (1984). Early life history stages of fishes and their characters. In *Ontogeny and Systematics of Fishes* (ed. H. G. Moser, W. J. Richards, D. M. Cohen, M. P. Fahay, J. A. W. Kendall and S. L. Richardson), pp. 11-22. Lawrence, KS: American Society of Ichthyologists and Herpetologists.
Kern, S. and Koumoutsakos, P. (2006). Simulations of optimized anguilliform swimming. *J. Exp. Biol.* **209**, 4841-4857.
Kingsford, M. J. and Tricklebank, K. A. (1991). Ontogeny and behavior of *Aldrichetta forsteri* (Teleostei: Mugilidae). *Copeia* **1991**, 9-16.
Lankheet, M. J., Stoffers, T., Van Leeuwen, J. L. and Pollux, B. J. A. (2016). Acquired versus innate prey capturing skills in super-precocial live-bearing fish. *Proc. R. Soc. B* **283**, 20160972.
Lee, W.-S., Monaghan, P. and Metcalfe, N. B. (2010). The trade-off between growth rate and locomotor performance varies with perceived time until breeding. *J. Exp. Biol.* **213**, 3289-3298.
Li, G., Müller, U. K., Van Leeuwen, J. L. and Liu, H. (2012). Body dynamics and hydrodynamics of swimming fish larvae: a computational study. *J. Exp. Biol.* **215**, 4015-4033.
Li, G., Müller, U. K., Van Leeuwen, J. L. and Liu, H. (2014). Escape trajectories are deflected when fish larvae intercept their own C-start wake. *J. R. Soc. Interface* **11**, 20140848-20140848.
Li, G., Müller, U. K., Van Leeuwen, J. L. and Liu, H. (2016). Fish larvae exploit edge vortices along their dorsal and ventral fin folds to propel themselves. *J. R. Soc. Interface* **13**, 20160068.
Lighthill, M. J. (1960). Note on the swimming of slender fish. *J. Fluid Mech.* **9**, 305-317.
Lighthill, M. J. (1971). Large-amplitude elongated-body theory of fish locomotion. *Proc. R. Soc. B* **179**, 125-138.
Liu, K. S. and Fetcho, J. R. (1999). Laser ablations reveal functional relationships of segmental hindbrain neurons in zebrafish. *Neuron* **23**, 325-335.
Liu, H., Wassersug, R. and Kawachi, K. (1997). The three-dimensional hydrodynamics of tadpole locomotion. *J. Exp. Biol.* **200**, 2807-2819.
Madan Mohan Rao, G. (1971). Influence of activity and salinity on the weight-dependent oxygen consumption of the rainbow trout *Salmo gairdneri*. *Mar. Biol.* **8**, 205-212.
Mascarello, F., Rowlerson, A., Radaelli, G., Scapolo, P.-A. and Veggetti, A. (1995). Differentiation and growth of muscle in the fish *Sparus aurata* (L): I. Myosin expression and organization of fibre types in lateral muscle from hatching to adult. *J. Muscle Res. Cell Motil.* **16**, 213-222.
McElligott, M. B. and O'Malley, D. M. (2005). Prey tracking by larval zebrafish: axial kinematics and visual control. *Brain Behav. Evol.* **66**, 177-196.
McHenry, M. J., Feitl, K. E., Strother, J. A. and Van Trump, W. J. (2009). Larval zebrafish rapidly sense the water flow of a predator's strike. *Biol. Lett.* **5**, 477-479.
McLean, D. L., Fan, J., Higashijima, S.-I., Hale, M. E. and Fetcho, J. R. (2007). A topographic map of recruitment in spinal cord. *Nature* **446**, 71-75.
McMillen, T. and Holmes, P. (2006). An elastic rod model for anguilliform swimming. *J. Math. Biol.* **53**, 843-886.
Mos, W. and Van der Stelt, A. (1982). Efficiency in relation to the design of the segmented body musculature in *Brachydanio rerio*. *Neth. J. Zool.* **32**, 123-143.
Müller, U. K. and Van Leeuwen, J. L. (2004). Swimming of larval zebrafish: ontogeny of body waves and implications for locomotory development. *J. Exp. Biol.* **207**, 853-868.
Müller, U. K., Van den Boogaart, J. G. M. and Van Leeuwen, J. L. (2008). Flow patterns of larval fish: undulatory swimming in the intermediate flow regime. *J. Exp. Biol.* **211**, 196-205.
Nair, A., Azatian, G. and McHenry, M. J. (2015). The kinematics of directional control in the fast start of zebrafish larvae. *J. Exp. Biol.* **218**, 3996-4004.
Nair, A., Nguyen, C. and McHenry, M. J. (2017). A faster escape does not enhance survival in zebrafish larvae. *Proc. R. Soc. B* **284**, 20170359.
Najafi, A. and Golestanian, R. (2004). Simple swimmer at low Reynolds number: Three linked spheres. *Phys. Rev. E Stat. Phys. Plasmas Fluids Relat. Interdiscip. Top.* **69**, 062901.
Omori, M., Sugawara, Y. and Honda, H. (1996). Morphogenesis in hatchery-reared larvae of the black rockfish, *Sebastes schlegeli*, and its relationship to the development of swimming and feeding functions. *Ichthyol. Res.* **43**, 267-282.
Osse, J. W. M. (1989). Form changes in fish larvae in relation to changing demands of function. *Neth. J. Zool.* **40**, 362-385.
Osse, J. W. M. and Van den Boogaart, J. G. M. (1995). Fish larvae, development, allometric growth, and the aquatic environment. *ICES Mar. Sci. Symp.* **201**, 21-34.
Osse, J. W. M. and Van den Boogaart, J. G. M. (1997). Size of flatfish larvae at transformation, functional demands and historical constraints. *J. Sea Res.* **37**, 229-239.
Osse, J. W. M. and Van den Boogaart, J. G. M. (2000). Body size and swimming types in carp larvae; effects of being small. *Neth. J. Zool.* **50**, 233-244.
Palstra, A., Van Ginneken, V. and Van den Thillart, G. (2008). Cost of transport and optimal swimming speed in farmed and wild European silver eels (*Anguilla anguilla*). *Comp. Biochem. Physiol. A Mol. Integr. Physiol.* **151**, 37-44.
Patterson, S. and Goldspink, G. (1976). Mechanism of myofibril growth and proliferation in fish muscle. *J. Cell Sci.* **22**, 607-616.
Peterson, I. and Wroblewski, J. S. (1984). Mortality rate of fishes in the pelagic ecosystem. *Can. J. Fish. Aquat. Sci.* **41**, 1117-1120.
Pottin, K., Hyacinthe, C. and Rétaux, S. (2010). Conservation, development, and function of a cement gland-like structure in the fish *Astyanax mexicanus*. *Proc. Natl. Acad. Sci. USA* **107**, 17256-17261.
Rome, L. C., Cook, C., Syme, D. A., Connaughton, M. A., Ashley-Ross, M., Klimov, A., Tikunov, B. and Goldman, Y. E. (1999). Trading force for speed: why superfast crossbridge kinetics leads to superlow forces. *Proc. Natl. Acad. Sci. USA* **96**, 5826-5831.

Ruzicka, J. J. and Gallager, S. M. (2006). The importance of the cost of swimming to the foraging behavior and ecology of larval cod (*Gadus morhua*) on Georges Bank. *Deep Sea Res. Part II Top. Stud. Oceanogr.* **53**, 2708-2734.
Sancho, G., Ma, D. and Lobel, P. (1997). Behavioral observations of an upcurrent reef colonization event by larval surgeonfish *Ctenochaetus strigosus* (Acanthuridae). *Mar. Ecol. Prog. Ser.* **153**, 311-315.
Scapolo, P. A., Veggetti, A., Mascarello, F. and Romanello, M. G. (1988). Developmental transitions of myosin isoforms and organisation of the lateral muscle in the teleost *Dicentrarchus labrax* (L.). *Anat. Embryol.* **178**, 287-295.
Schmidt-Nielsen, K. (1972). Locomotion: energy cost of swimming, flying, and running. *Science* **177**, 222-228.
Schultz, W. W. and Webb, P. W. (2002). Power requirements of swimming: do new methods resolve old questions? *Integr. Comp. Biol.* **42**, 1018-1025.
Seebacher, F., Elsworth, P. G. and Franklin, C. E. (2003). Ontogenetic changes of swimming kinematics in a semi-aquatic reptile (*Crocodylus porosus*). *Aust. J. Zool.* **51**, 15-24.
Sogard, S. M. (1997). Size-selective mortality in the juvenile stage of teleost fishes: a review. *Bull. Mar. Sci.* **60**, 1129-1157.
Spierts, I. L. Y. (2001). Titin isoforms and kinematics of fast swimming carp larvae (*Cyprinus carpio* L.). *Neth. J. Zool.* **51**, 17-31.
Stewart, W. J., Cardenas, G. S. and McHenry, M. J. (2013). Zebrafish larvae evade predators by sensing water flow. *J. Exp. Biol.* **216**, 388-398.
Stewart, W. J., Nair, A., Jiang, H. and McHenry, M. J. (2014). Prey fish escape by sensing the bow wave of a predator. *J. Exp. Biol.* **217**, 4328-4336.
Taylor, G. K., Nudds, R. L. and Thomas, A. L. R. (2003). Flying and swimming animals cruise at a Strouhal number tuned for high power efficiency. *Nature* **425**, 707-711.
Triantafyllou, G. S., Triantafyllou, M. S. and Grosenbaugh, M. A. (1993). Optimal thrust development in oscillating foils with application to fish propulsion. *J. Fluids Struct.* **7**, 205-224.
Tytell, E. D. and Lauder, G. V. (2008). Hydrodynamics of the escape response in bluegill sunfish, *Lepomis macrochirus*. *J. Exp. Biol.* **211**, 3359-3369.
Tytell, E. D., Hsu, C.-Y., Williams, T. L., Cohen, A. H. and Fauci, L. J. (2010). Interactions between internal forces, body stiffness, and fluid environment in a neuromechanical model of lamprey swimming. *Proc. Natl. Acad. Sci. USA* **107**, 19832-19837.
Unal, M. F., Lin, J.-C. and Rockwell, D. (1997). Force prediction by PIV imaging: a momentum-based approach. *J. Fluids Struct.* **11**, 965-971.
Van der Meulen, T., Schipper, H., Van Leeuwen, J. L. and Kranenbarg, S. (2005). Effects of decreased muscle activity on developing axial musculature in *nic^{b107}* mutant zebrafish (*Danio rerio*). *J. Exp. Biol.* **208**, 3675-3687.
Van Leeuwen, J. L. (1984). A quantitative study of flow in prey capture by rainbow trout, *Salmo gairdneri* with general consideration of the actinopterygian feeding mechanism. *Trans. Zool. Soc. London* **37**, 171-227.
Van Leeuwen, J. L., Lankheet, M. J. M., Akster, H. A. and Osse, J. W. M. (1990). Function of red axial muscles of carp (*Cyprinus carpio*): recruitment and normalized power output during swimming in different modes. *J. Zool.* **220**, 123-145.
Van Leeuwen, J. L., Van der Meulen, T., Schipper, H. and Kranenbarg, S. (2008). A functional analysis of myotomal muscle-fibre reorientation in developing zebrafish *Danio rerio*. *J. Exp. Biol.* **211**, 1289-1304.
Van Leeuwen, J. L., Voesenek, C. J. and Müller, U. K. (2015a). Data from: How body torque and Strouhal number change with swimming speed and developmental stage in larval zebrafish. *Dryad Digital Repository*.
Van Leeuwen, J. L., Voesenek, C. J. and Müller, U. K. (2015b). How body torque and Strouhal number change with swimming speed and developmental stage in larval zebrafish. *J. R. Soc. Interface* **12**, 20150479.
Veggetti, A., Mascarello, F., Scapolo, P. A., Rowlerson, A. and Candia Carnevali, M. D. C. (1993). Muscle growth and myosin isoform transitions during development of a small teleost fish, *Poecilia reticulata* (Peters) (Atheriniformes, Poeciliidae): a histochemical, immunohistochemical, ultrastructural and morphometric study. *Anat. Embryol.* **187**, 353-361.
Verhagen, J. H. G. (2004). Hydrodynamics of burst swimming fish larvae; a conceptual model approach. *J. Theor. Biol.* **229**, 235-248.
Vieira, V. I. A. and Johnston, I. A. (1992). Influence of temperature on muscle-fibre development in larvae of the herring *Clupea harengus*. *Mar. Biol.* **112**, 333-341.
Voesenek, C. J., Pieters, R. P. M. and Van Leeuwen, J. L. (2016). Automated reconstruction of three-dimensional fish motion, forces, and torques. *PLoS ONE* **11**, e0146682.
Wakeling, J. M., Kemp, K. M. and Johnston, I. A. (1999). The biomechanics of fast-starts during ontogeny in the common carp *Cyprinus carpio*. *J. Exp. Biol.* **202**, 3057-3067.
Ware, D. M. (1975). Growth, metabolism, and optimal swimming speed of a pelagic fish. *J. Fish. Res. Board Can.* **32**, 33-41.
Webb, P. W. (1984). Body and fin form and strike tactics of four teleost predators attacking fathead minnow (*Pimephales promelas*) prey. *Can. J. Fish. Aquat. Sci.* **41**, 157-165.
Webb, P. W., Kostecki, P. T. and Don Stevens, E. (1984). The effect of size and swimming speed on locomotor kinematics of rainbow trout. *J. Exp. Biol.* **109**, 77-95.
Weihs, D. (1979). Energetic significance of changes in swimming modes during growth of larval anchovy, *Engraulis mordax*. *Fish. Bull.* **77**, 597-604.
Wieser, W. (1995). Energetics of fish larvae, the smallest vertebrates. *Acta Physiol. Scand.* **154**, 279-290.
Wilson, D. M. (1959). Function of giant Mauthner's neurons in the lungfish. *Science* **129**, 841-842.
Xiong, G. and Lauder, G. V. (2014). Center of mass motion in swimming fish: effects of speed and locomotor mode during undulatory propulsion. *Zoology* **117**, 269-281.